Hindawi
Complexity
Volume 2018, Article ID 4159639, 16 pages
https://doi.org/10.1155/2018/4159639

Research Article

RBF Neural Network Backstepping Sliding Mode Adaptive Control for Dynamic Pressure Cylinder Electrohydraulic Servo Pressure System

Pan Deng,[1,2] Liangcai Zeng,[1] and Yang Liu[2]

[1] *School of Machinery and Automation, Wuhan University of Science and Technology, Wuhan 430081, China*
[2] *Wuhan Branch of Baosteel Central Research Institute (R&D Center of Wuhan Iron & Steel Co., Ltd.), Wuhan 430081, China*

Correspondence should be addressed to Pan Deng; dengpan390@126.com

Received 27 August 2018; Revised 19 October 2018; Accepted 11 November 2018; Published 2 December 2018

Academic Editor: Carlos F. Aguilar-Ibáñez

According to the hydraulic principle diagram of the subgrade test device, the dynamic pressure cylinder electrohydraulic servo pressure system math model and AMESim simulation model are established. The system is divided into two parts of the dynamic pressure cylinder displacement subsystem and the dynamic pressure cylinder output pressure subsystem. On this basis, a RBF neural network backstepping sliding mode adaptive control algorithm is designed: using the double sliding mode structure, the two RBF neural networks are used to approximate the uncertainties in the two subsystems, provide design methods of RBF sliding mode adaptive controller of the dynamic pressure cylinder displacement subsystem and RBF backstepping sliding mode adaptive controller of the dynamic pressure cylinder output pressure subsystem, and give the two RBF neural network weight vector adaptive laws, and the stability of the algorithm is proved. Finally, the algorithm is applied to the dynamic pressure cylinder electrohydraulic servo pressure system AMESim model; simulation results show that this algorithm can not only effectively estimate the system uncertainties, but also achieve accurate tracking of the target variables and have a simpler structure, better control performance, and better robust performance than the backstepping sliding mode adaptive control (BSAC).

1. Introduction

The track subgrade dynamic response test device is mainly used to simulate the comprehensive impact of high-speed running trains on the subgrade. The constant pressure of static pressure cylinder is set by the pilot type electrohydraulic proportional pressure reducing valve to simulate the static load generated by the train's own weight on the subgrade; the alternating hydraulic pressure is applied to the dynamic pressure cylinder through the servo valve to simulate the dynamic load on the subgrade during the train high-speed running [1–3]. The hydraulic schematic diagram of the track subgrade test device is shown in Figure 1. The dynamic pressure cylinder piston rod outputs an alternating dynamic load, obtaining the resultant load force by superimposing the static load of the static pressure piston rod, and finally, the loading force is loaded on the tested subgrade through the sensor and the excitation block. Therefore, the dynamic pressure cylinder system is a typical electrohydraulic servo pressure system.

The control performance of the composite loading force depends on the precise control of the dynamic pressure cylinder electrohydraulic servo pressure system, because the dynamic pressure cylinder electrohydraulic servo pressure system has the parameter uncertainty and flow nonlinearity, which increase the difficulty of the control system design. The backstepping control constructs the Lyapunov function at all levels, selects the intermediate virtual control quantity at each level according to the design goals, and obtains the control law of the system by step backward recursion; it is a feedback control method based on the Lyapunov stability theory [4, 5]. Sliding mode variable structure control has the advantages of high control precision and simple structure, can greatly reduce the influence of system nonlinearity, and has strong robustness [6, 7]. Adaptive control is often used to reduce the impact of parameter uncertainty on system

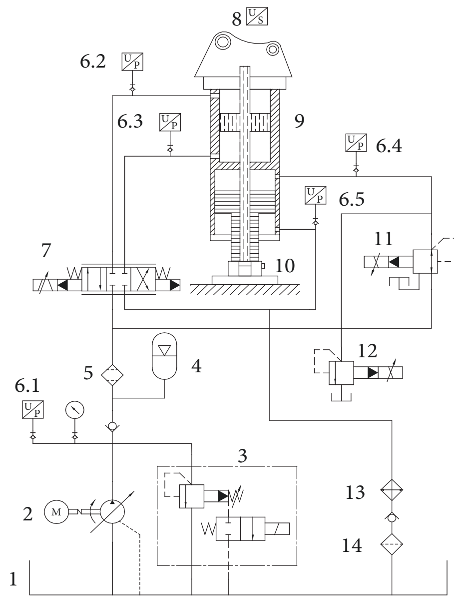

Figure 1: The hydraulic schematic diagram of the track subgrade test device. (1) Oil tank. (2) Constant pressure variable pump. (3) Safety valve. (4) Accumulator. (5) Inlet filter. (6) Hydraulic pressure sensor. (7) Servo valve. (8) Displacement sensor. (9) Double-ring servo cylinder. (10) Load sensor. (11) Three-way proportional pressure reducing valve. (12) Electromagnetic overflow valve. (13) Cooler. (14) Oil return filter.

performance [8–10]. Therefore, backstepping sliding mode adaptive control has been widely used in electromechanical servo control [11–13], electrohydraulic servo control [14–16], flight navigation control [17, 18], and other fields, achieving good control effects.

In the actual system, the external interference is unknown, and the system still has modeling errors. Therefore, the upper bounds of uncertainties in the system are often difficult to determine. The uncertainty boundary problem has become an important part of controller design, which directly affects the performance of the whole control system. In recent years, with the development of intelligent control theory, neural networks with their good approximation characteristics have been widely used in the estimation of unknown parts of the system and have achieved good results. Xu Chuanzhong [19] designed the RBF neural network adaptive law to estimate the upper bound of uncertain factors in the backstepping sliding mode control system, thus improving the robustness of the system to factors such as modeling errors and uncertain disturbances. Chen Ziyin [20] compensated the model uncertainty in the pitch motion of underwater vehicles through a neural network controller and designed an adaptive robust controller to eliminate the approximation error of the neural network.

In order to achieve rapid and accurate pressure tracking control of dynamic pressure cylinder electrohydraulic servo pressure system, this paper designed a RBF neural network backstepping sliding mode adaptive control method, which can effectively reduce the influence of system uncertainties and nonlinearities, so that the system output pressure has good tracking performance and robust performance.

2. Model of Dynamic Pressure Cylinder Electrohydraulic Servo Pressure System

2.1. Mathematical Model. The dynamic pressure cylinder electrohydraulic servo pressure control system mainly includes control signal, servo amplifier, servo valve, dynamic pressure cylinder, sensor, and load.

The servo valve system includes the spool equation and the flow equation:

$$X_V = K_S G_{SV} U_e \tag{1}$$

$$Q_L = C_d \omega X_V \sqrt{\frac{1}{\rho}\left(P_S - \operatorname{sign}\left(X_V\right) P_L\right)} \tag{2}$$

where X_V is the servo valve spool displacement, K_S is the servo valve system overall gain, G_{SV} is the servo valve transfer function at unity gain, U_e is the servo amplifier input voltage signal, Q_L is the servo valve output flow, C_d is the servo valve port flow coefficient, ω is the servo valve main spool area gradient, P_S is the system supply pressure, P_L is the load pressure, and ρ is the oil density.

Since the natural frequency of the servo valve is close to the hydraulic frequency of the dynamic hydraulic cylinder, this paper uses the second-order oscillation element to describe the servo valve transfer function [21] and retain the flow nonlinear part of the servo valve. The description of the load flow is as follows:

$$Q_L = G_{SVK} U_e g(u) = \frac{a_{81} U_e g(u)}{S^2 + a_6 S + a_7} \tag{3}$$

where a_6, a_7, a_{81} are the servo coefficients and $g(u) = \sqrt{P_S - \operatorname{sign}(u) P_L}$ is the flow nonlinear part.

Dynamic pressure cylinder can be described as

$$Q_L = A_P S X_m + C_{tp} P_L + \frac{V_m}{4\beta_e} S P_L \tag{4}$$

$$A_P P_L + F_L = m S^2 X_m + B_m S X_m + K X_m \tag{5}$$

where m is the mass of dynamic pressure cylinder vibration system, B_m is the load damping coefficient, K is the subgrade elastic stiffness, F_L is the static load of static pressure cylinder, A_p is the effective area of dynamic pressure cylinder piston, C_{tp} is the dynamic pressure cylinder total leakage coefficient, V_m is the system pipe total compression volume, and β_e is the effective volumetric elastic modulus of hydraulic oil.

Combining (4) and (5), using static load F_L and servo valve output flow Q_L as input variables, and selecting dynamic pressure cylinder displacement, speed, and output pressure

P_L as state variables, the state equation of the dynamic pressure cylinder can be obtained as follows:

$$\begin{aligned} \dot{x}_1 &= x_2 \\ \dot{x}_2 &= -a_1x_1 - a_2x_2 + a_3x_3 + a_fF_L \\ \dot{x}_3 &= -a_4x_2 - a_5x_3 + b_1Q_L \end{aligned} \tag{6}$$

where X_1 is the dynamic pressure cylinder displacement, X_2 is the dynamic pressure cylinder speed, X_3 is the dynamic pressure cylinder output pressure, $a_1 = K/m$, $a_2 = B/m$, $a_3 = A_p/m$, $a_4 = 4A_p\beta_e/V_m$, $a_5 = 4C_{tp}\beta_e/V_m$, $a_f = 1/m$, $b_1 = 4\beta_e/V_m$.

Substituting (3) into the third item of (6), introducing the target variable P_r into the state variable, and letting $\xi_1 = X_1$, $\xi_2 = X_2$, $\xi_3 = P_r$-X_3, $\xi_4 = \dot{\xi}_3 = \dot{P}_r - x_4$, $\xi_5 = \dot{\xi}_4 = \ddot{P}_r - x_5$, (6) can be transformed to

$$\begin{aligned} \dot{\xi}_1 &= \xi_2 \\ \dot{\xi}_2 &= -a_1\xi_1 - a_2\xi_2 - a_3\xi_3 + a_3P_r + a_fF_L + \Delta_1 \\ \dot{\xi}_3 &= \xi_4 \\ \dot{\xi}_4 &= \xi_5 \\ \dot{\xi}_5 &= -a_{21}\xi_1 + a_{20}\xi_2 - a_{19}\xi_3 - a_{18}\xi_4 - a_9\xi_5 + P_{Pr} + F_{FL} \\ &\quad + \Delta_2 - a_8g(u)u \end{aligned} \tag{7}$$

where $a_8 = a_{81}b_1$, $a_9 = a_5 + a_6$, $a_{10} = a_7 + a_5a_6$, $a_{11} = a_5a_7$, $a_{12} = a_4a_6$, $a_{13} = a_4a_7$, $a_{14} = a_{12}$-a_2a_4, $a_{15} = a_{13}$-a_1a_4, $a_{16} = a_3a_4$, $a_{17} = a_fa_4$, $a_{18} = a_{10}$-a_{16}, $a_{19} = a_{11} + a_3a_{14}$, $a_{21} = a_1a_{14}$, $a_{22} = a_fa_{14}$, $a_{20} = a_{15}$-a_2a_{14}, $F_{FL} = a_{22}F_L + a_{17}\dot{F}_L$, $P_{Pr} = a_{19}P_r + a_{18}\dot{P}_r + a_9\ddot{P}_r + \dddot{P}_r$, $\Delta_1 = -da_1\xi_1 - da_2\xi_2 + da_3(P_r - \xi_3) + d_1$ $\Delta_2 = da_{21}\xi_1 - da_{20}\xi_2 + da_{19}(\xi_3 - P_r) + da_{18}(\xi_4 - \dot{P}_r) + da_9(\xi_5 - \ddot{P}_r) + d_2$.

The external disturbance is much smaller than the static load F_L(150KN). Therefore, ignoring the influence of external interference, the static load F_L is equivalent to an external disturbance, being constant and bounded.

2.2. AMESim and Simulink Cosimulation Model. It can be seen from the hydraulic schematic diagram Figure 1 of the track subgrade test device that the dynamic pressure cylinder electrohydraulic servo pressure control system mainly includes dynamic pressure cylinder, flow servo valve, and sensor. The dynamic pressure cylinder electrohydraulic servo pressure system AMESim and Simulink cosimulation model is established as Figure 2.

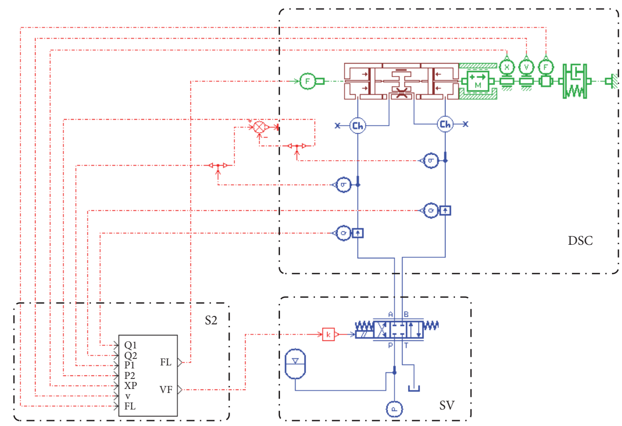

Figure 2: Dynamic pressure cylinder electrohydraulic servo pressure system AMESim and Simulink cosimulation model.

3. Backstepping Sliding Mode Controller Design

3.1. System Decomposition. The dynamic pressure cylinder electrohydraulic servo pressure system described in (7) can be divided into two parts: the dynamic pressure cylinder displacement subsystem and the dynamic pressure cylinder output pressure subsystem.

Dynamic pressure cylinder displacement subsystem:

$$\begin{aligned} \dot{\xi}_1 &= \xi_2 \\ \dot{\xi}_2 &= -a_1\xi_1 - a_2\xi_2 - a_3\xi_3 + a_3P_r + a_fF_L + \Delta_1 \end{aligned} \tag{8}$$

Dynamic pressure cylinder output pressure subsystem:

$$\begin{aligned} \dot{\xi}_3 &= \xi_4 \\ \dot{\xi}_4 &= \xi_5 \\ \dot{\xi}_5 &= -a_{21}\xi_1 + a_{20}\xi_2 - a_{19}\xi_3 - a_{18}\xi_4 - a_9\xi_5 + P_{Pr} + F_{FL} \\ &\quad - a_8g(u)u + \Delta_2 \end{aligned} \tag{9}$$

3.2. Dynamic Pressure Cylinder Displacement Subsystem Sliding Mode Control. According to (8) description, ξ_{d1} is set as the expected displacement of the dynamic pressure cylinder displacement subsystem; define the displacement tracking error as $e_1 = \xi_1$-ξ_{d1}, and construct the sliding mode switch function of displacement subsystem as follows:

$$S_1 = c_1e_1 + c_2\dot{e}_1 \tag{10}$$

where c_1, c_2 are switching function coefficients, positive real numbers.

Taking the derivative of sliding mode switching functions S_1 and substituting (8) into $\dot{S}_1$, we can get

$$\begin{aligned} \dot{S}_1 &= C_1\dot{e}_1 + C_2\ddot{e}_1 = C_1\dot{\xi}_1 + C_2\dot{\xi}_2 - C_1\dot{\xi}_{d1} - C_2\ddot{\xi}_{d1} \\ &= C_1\xi_2 \\ &\quad + C_2\left(-a_1\xi_1 - a_2\xi_2 - a_3\xi_3 + a_3 + a_fF_L + \Delta_1\right) \\ &\quad - \xi dd \\ &= -aa_1\xi_1 - aa_2\xi_2 - aa_3\xi_3 + aa_3P_r + aa_4F_L + C_2\Delta_1 \\ &\quad - \xi dd \end{aligned} \tag{11}$$

where $aa_1 = c_2a_1$, $aa_2 = c_2a_2\text{-}c_1$, $aa_3 = c_2a_3$, $aa_4 = c_2a_f$, $\xi dd = C_1\dot{\xi}_{d1} + C_2\ddot{\xi}_{d1}$.

Let ξ_{d3} be the expected variable of the displacement subsystem variable ξ_3, and then its tracking error $e_{31} = \xi_3\text{-}\xi_{d3}$; the expectation ξ_{d3} of this paper is $\xi_{d3} = 0$, so $e_{31} = \xi_3$, and ξ_3 is replaced by a virtual output control variable e_{31}. Assuming that the above parameters and uncertainties are known, we can obtain the virtual controller as follows [22].

$$\begin{aligned} e_{31} = \frac{1}{aa_3} & \left(-aa_1\xi_1 - aa_2\xi_2 + aa_3P_r + aa_4F_L + C_2\Delta_1\right. \\ & \left.- \xi dd - K_1S_1\right) \end{aligned} \tag{12}$$

3.3. Dynamic Pressure Cylinder Output Pressure Subsystem Backstepping Sliding Mode Control. Set ξ_{d3} as the expected output pressure of the dynamic pressure cylinder output pressure subsystem, and the tracking error of the output pressure is $e_3 = \xi_3\text{-}\xi_{d3}$; use backstepping algorithm, combined with (9), to gradually derive the virtual control variables at all levels as follows.

Step 1. Construct Lyapunov function as $V_3 = (1/2)K_3K_4e_3^2$ and derivative

$$\dot{V}_3 = K_3K_4e_3\dot{e}_3 = K_3K_4e_3\left(\xi_4 - \dot{\xi}_{d3}\right) \tag{13}$$

Let the derivative of tracking error e_3 be $e_4 = \xi_4\text{-}\xi_{4d}$, and take the virtual control variable ξ_{4d} as

$$\xi_{4d} = e_3 - \dot{\xi}_{d3}. \tag{14}$$

Substituting (14) into (13), we can get

$$\dot{V}_3 = -K_3K_4e_3^2 + K_3K_4e_3e_4 \tag{15}$$

Step 2. Construct the Lyapunov function as $V_4 = V_3 + (1/2)K_3K_4K_5e_4^2$ and derivative

$$\begin{aligned} \dot{V}_4 &= \dot{V}_3 + K_3K_4K_5e_4\dot{e}_4 \\ &= -K_3K_4e_3^2 + K_3K_4e_4\left(\xi_5 - \dot{\xi}_{4d}\right) \end{aligned} \tag{16}$$

Let the derivative of $\dot{e}_3$ be $e_5 = \xi_5\text{-}\xi_{5d}$, and take the virtual control variable ξ_{5d} as

$$\xi_{5d} = -e_4 + \frac{(-e_4 - e_3)}{K_5} + \dot{\xi}_{4d} \tag{17}$$

Substituting (17) into (16), we can get

$$\dot{V}_4 = -K_3K_4e_3^2 - K_3K_4K_5e_4^2 - K_3K_4e_4\left(e_4 - K_5e_5\right) \tag{18}$$

where K_3, K_4, K_5 are Lyapunov function coefficients, positive real numbers.

Step 3. Design the sliding mode switching function of the dynamic pressure cylinder output pressure subsystem as

$$S_2 = c_3e_3 + c_4e_4 + c_5e_5 \tag{19}$$

where c_3, c_4, c_5 are switching function coefficients, positive real numbers.

Substituting (9) into $\dot{S}_2$, we can get

$$\begin{aligned} \dot{S}_2 &= C_3\dot{e}_3 + C_4\dot{e}_4 + C_5\dot{e}_5 \\ &= C_3\left(\dot{\xi}_3 - \dot{\xi}_{3d}\right) + C_4\left(\dot{\xi}_4 - \dot{\xi}_{4d}\right) + C_5\left(\dot{\xi}_5 - \dot{\xi}_{5d}\right) \\ &= C_3\xi_4 + C_4\xi_5 + C_5\dot{\xi}_5 - \xi dd1 \\ &= -aa_5\xi_1 + aa_6\xi_2 - aa_7\xi_3 - aa_8\xi_4 - aa_9\xi_5 \\ &\quad + aa_{10}F_L - aa_{11}g(u)u + C_5P_{P_r} + \xi dd1 + C_5\Delta_2 \end{aligned} \tag{20}$$

where $aa_5 = c_5a_{21}$, $aa_6 = c_5a_{20}$, $aa_7 = c_5a_{19}$, $aa_8 = c_5a_{18} - c_3$, $aa_9 = c_5a_9 - c_4$, $aa_{10} = c_5a_{22}$, $aa_{11} = c_5a_8$, $\xi dd1 = c_3\dot{\xi}_{d3} + c_4\dot{\xi}_{4d} + c_5\dot{\xi}_{5d}$.

Let $\dot{S}_2 = 0$; the expression of the backstepping sliding mode controller of the dynamic pressure cylinder output pressure subsystem can be obtained:

$$\begin{aligned} u = \frac{1}{aa_{11}g(u)} & \left(-aa_5\xi_1 + aa_6\xi_2 - aa_7\left(\xi_3 - P_r\right)\right. \\ & - aa_8\left(\xi_4 - \dot{P}_r\right) + PP - aa_9\left(\xi_5 - \ddot{P}_r\right) + aa_{10}F_L \\ & \left.- \xi dd1 + C_5\Delta_2\right) \end{aligned} \tag{21}$$

where $PP = c_3\dot{P}_r + c_4\ddot{P}_r + c_5\dddot{P}_r$.

3.4. The Selection of the Expected Displacement ξ_{d1} of the Displacement Subsystem. When the dynamic pressure cylinder displacement subsystem is stable, the displacement tracking error e_1 is very small, at this time, $\xi_1 \approx \xi_{d1}$. Since $aa_1 >> aa_2$, $aa_1 >> c_1$, and $aa_1 >> c_2$, according to the virtual controller (12), combined with the expected output pressure ξ_{d3}, the desired displacement ξ_{d1} of the dynamic pressure cylinder can be expressed approximately as follows:

$$\xi_{d1} \approx \frac{1}{aa_1}\left(aa_3\left(P_r - \xi_{d3}\right) + aa_4F_L\right) \tag{22}$$

The virtual control variable e_{31} is used to implement the tracking control of (22); with the premise of good displacement tracking performance, we expect e_{31} to be as small as possible. However, e_{31} may be relatively large in actual operation, resulting in a large difference in displacement ξ_1 between (8) and (7); thus it has some influence on the dynamic pressure cylinder output pressure subsystem. Because the two subsystems independently carry out the stability design, the above mentioned differences between the e_{31} and e_3 will not affect the stability of the whole system, and the final output pressure tracking performance is only related to the design of the virtual controller (12) and the backstepping sliding mode controller (21).

4. RBF Neural Network Backstepping Sliding Mode Adaptive Controller Design

4.1. Dynamic Pressure Cylinder Displacement Subsystem RBF NN Sliding Mode Adaptive Control. The dynamic pressure cylinder displacement subsystem described by (8) constructs the displacement subsystem sliding mode switching function such as (10); let $f_1 = C_2\Delta_1$, and (11) can be expressed as

$$\dot{S}_1 = -aa_1\xi_1 - aa_2\xi_2 - aa_3\xi_3 + aa_3P_r + aa_4F_L + f_1 - \xi dd \tag{23}$$

4.1.1. RBF NN Approximation for Uncertainty of Dynamic Pressure Cylinder Displacement Subsystem. Using the good approximation performance of the RBF neural network, estimate the uncertainty term $f_1$of the dynamic pressure cylinder displacement subsystem, which can effectively solve the problem that the upper bound of the uncertain term is difficult to determine.

$$\widehat{f}_1(\xi_v) = \sum_{j=1}^{l}\widehat{w_j}h_j(\xi_v) = \widehat{W^T}h(\xi_v) \tag{24}$$

where $\widehat{W^T}$ is the weight vector of the RBF, $\widehat{W^T} = [\widehat{w_1}, \widehat{w_2}, \ldots, \widehat{w_l}]$; $h(\xi_v)$ is the radial basis vector of the RBF, $h(\xi_v) = [h_1(\xi_v), h_2(\xi_v), \ldots, h_l(\xi_v)]^T$, l is the number of hidden layer nodes.

And $h_j(\xi_v)$ is a Gaussian function with the following expression:

$$h_j(\xi_v) = \exp\left(\frac{\|X - C_j\|^2}{2b_j^2}\right), \quad j = 1, 2, \ldots, l \tag{25}$$

where $C_j = [c_{1j}, c_{2j}]^{\mathrm{T}}$ is the central vector of the jth network node; b_j is the base width parameter of the jth network node.

Assumption 1. Using the RBF neural network to approximate the uncertain term $f_1(\xi_v)$, there is an optimal weight $Wb = \arg\min_{W\in R^l}(\sup|\widehat{W^T}h(\xi_v) - f_1(\xi_v)|)$ to make the neural network approximation error $\varepsilon(\xi_v)$ to satisfy $Wb^Th(\xi_v) - \overline{f}_1 = \varepsilon(\xi_v)$, and $\|\varepsilon(\xi_v)\| \le \varepsilon_b$, where $\overline{f}_1$ is the upper bound of the uncertainty of $f_1(\xi_v)$; i.e., $\overline{f}_1 - \|f_1(\xi_v)\| > \varepsilon_1 > \varepsilon_b$.

The uncertain term f_1 in (23) is estimated by the RBF neural network of (24); the adaptive virtual controller of the sliding mode RBF neural network of the dynamic cylinder displacement subsystem can be obtained:

$$e_{32} = \frac{1}{aa_3}\left(-aa_1\xi_1 - aa_2\xi_2 + aa_3P_{\mathrm{r}} + aa_4F_L + \widehat{W^T}h(\xi_v) - \xi dd\right) \tag{26}$$

4.1.2. Design of RBF NN Sliding Mode Adaptive Controller. The boundary layer method is introduced to reduce chattering near the sliding surface [23, 24], and the adaptive virtual controller is modified to

$$e_{31} = e_{32} + K_1 sat\left(\frac{S_1}{\varphi_1}\right) \tag{27}$$

where K_1 is the switching gain, and its adaptive law is designed as $\dot{K}_1 = K_{11}|S_1|$, K_{11} is a positive real number;

$$sat\left(\frac{S_1}{\varphi_1}\right) = \begin{cases} \dfrac{S_1}{\varphi_1}, & |S_1| \le \varphi_1 \\ \operatorname{sgn}(S_1), & |S_1| > \varphi_1 \end{cases} \tag{28}$$

is the boundary function.

Furthermore, the weight vector adaptive law of the displacement subsystem RBF neural network is

$$\dot{\widehat{W}} = \eta_1 h(\xi_v)S_1 - \delta_1\widehat{W} \tag{29}$$

where δ_1 is the weight vector correction coefficient, which can reduce the weight vector size and prevent the controller gain saturation, thus improving the robustness of the neural network approximation error [25] and satisfying $\delta_1 > 0$.

4.2. Dynamic Pressure Cylinder Output Pressure Subsystem RBF NN Backstepping Sliding Mode Adaptive Control. Let $f_2 = C_5\Delta_2$; (20) can be expressed as

$$\dot{S}_2 = -aa_5\xi_1 + aa_6\xi_2 - aa_7\xi_3 - aa_8\xi_4 - aa_9\xi_5 + aa_{10}F_L - aa_{11}g(u)u + C_5P_{P_r} + \xi dd + f_2 \tag{30}$$

4.2.1. RBF NN Approximation for Uncertainty of Dynamic Pressure Cylinder Output Pressure Subsystem. $f_2$is the uncertainty term of the dynamic pressure cylinder output pressure subsystem, and its RBF neural network approximator is as follows:

$$\widehat{f}_2(\xi_p) = \sum_{n=1}^{m}\widehat{p_n}\phi_n(\xi_p) = \widehat{P^T}\phi(\xi_p) \tag{31}$$

where m is the number of hidden layer nodes; $\xi_p = [\xi_3, \xi_4, \xi_5]^{\mathrm{T}}$ is input vector of the RBF; $\widehat{P^T}$ is the weight vector of the RBF, $\widehat{P^T} = [\widehat{p_1}, \widehat{p_2}, \ldots, \widehat{p_m}]$; $\phi(\xi_p)$ is the radial basis vector of the RBF, $\phi(\xi_p) = [\phi_1(\xi_p), \phi_2(\xi_p), \ldots, \phi_m(\xi_p)]^T$.

And $\Phi_n(\xi_p)$ is a Gaussian function with the following expression:

$$\phi_n(\xi_p) = \exp\left(\frac{\|X - CP_n\|^2}{2bP_n^2}\right), \quad n = 1, 2, \ldots, m \tag{32}$$

where $CP_n = [cp_{1n}, cp_{2n}, cp_{3n}]^{\mathrm{T}}$ is the central vector of the nth network node; bp_n is the base width parameter of the nth network node.

Assumption 2. Using the RBF neural network to approximate the uncertain term $f_2(\xi_p)$, there is an optimal weight

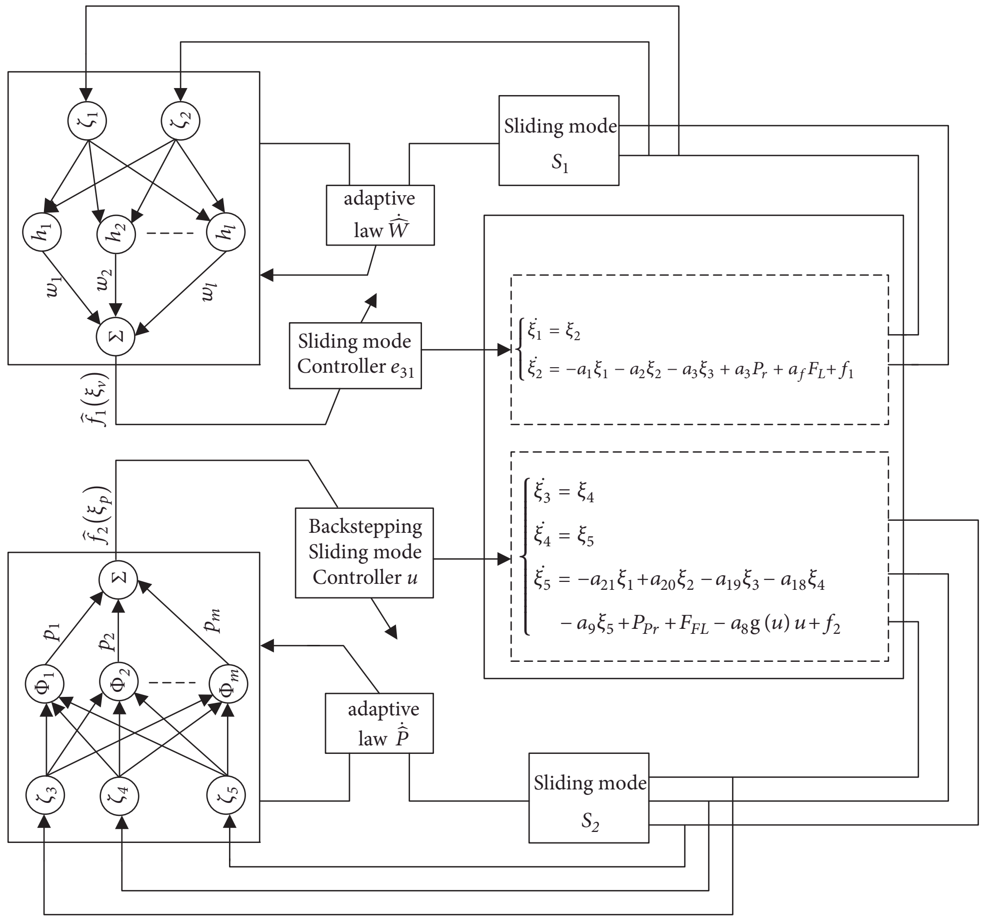

FIGURE 3: Dynamic pressure cylinder electrohydraulic servo pressure system RBF neural network backstepping sliding mode adaptive control block diagram.

$Pb = \arg\min_{W\in R^m}(\sup|\widehat{P^T}\phi(\xi_P) - f_2(\xi_P)|)$; make the neural network approximation error $\beta(\xi_P)$ to satisfy $Pb^T\Phi(\xi_P) - \overline{f}_2 = \beta(\xi_P)$, and $\|\beta(\xi_v)\| \le \beta_b$, where $\overline{f}_2$ is the upper bound of the uncertainty of $f_2(\xi_P)$; i.e., $\overline{f}_2 - \|f_2(\xi_P)\| > \beta_1 > \beta_b$.

Then we can obtain the RBF neural network backstepping sliding mode adaptive controller of the dynamic pressure cylinder output pressure subsystem:

$$\begin{aligned} u_1 = {} & \frac{1}{aa_{11}g(u)}\Big(-aa_5\xi_1 + aa_6\xi_2 - aa_7(\xi_3 - P_r) \\ & - aa_8(\xi_4 - \dot{P}_r) + PP - aa_9(\xi_5 - \ddot{P}_r) + aa_{10}F_L \\ & + \widehat{P^T}\phi(\xi_p) - \xi dd1\Big) \end{aligned} \quad (33)$$

4.2.2. Design of RBF NN Backstepping Sliding Mode Adaptive Controller. Using the boundary layer method, the controller is as follows:

$$u = u_1 + K_2 sat\left(\frac{S_2}{\varphi_2}\right) \quad (34)$$

where K_2 is the switching gain, and its adaptive law is designed as $\dot{K}_2 = K_{22}|S_2|$, K_{22} is a positive real number;

$$sat\left(\frac{S_2}{\varphi_2}\right) = \begin{cases} \dfrac{S_2}{\varphi_2}, & |S_2| \le \varphi_2 \\ \operatorname{sgn}(S_2), & |S_2| > \varphi_2 \end{cases} \quad (35)$$

is the boundary function.

The weight vector adaptive law of the output pressure subsystem RBF neural network is

$$\dot{\hat{P}} = \eta_2\phi(\xi_P)S_2 - \delta_2\hat{P} \quad (36)$$

where δ_2 is the weight vector correction coefficient, satisfying $\delta_2 > 0$.

4.3. Design and Stability Analysis of RBF Neural Network Backstepping Sliding Mode Adaptive Control for the Dynamic Pressure Cylinder Electrohydraulic Servo Pressure System

4.3.1. Design of RBF Neural Network Backstepping Sliding Mode Adaptive Control. Figure 3 is the control structure block diagram of the dynamic pressure cylinder electrohydraulic servo pressure system RBF neural network backstepping sliding mode adaptive control. In Figure 3, the dynamic pressure cylinder system consists of the displacement subsystem described by (8) and the output pressure subsystem described by (9); two RBF neural networks ($\widehat{f}_1(\xi_v)$ and $\widehat{f}_2(\xi_p)$) and their adaptive laws ($\dot{\widehat{W}}$ and $\dot{\widehat{P}}$) are used to approximate the subsystem uncertainties $f_1(\xi_v)$ and $f_2(\xi_P)$ and realize the tracking control of the output pressure of the dynamic pressure cylinder by separately constructing the virtual controller e_{31} and the pressure controller u.

Furthermore, the dynamic pressure cylinder RBF neural network backstepping sliding mode adaptive control system can be constructed by Theorem 3.

Theorem 3. *The dynamic pressure cylinder electrohydraulic servo pressure system described in (7) can be decomposed into the dynamic pressure cylinder displacement subsystem described in (8) and the dynamic pressure cylinder output pressure subsystem described in (9); the dynamic pressure cylinder displacement subsystem adopts the sliding mode switching function of (10), uses RBF neural network described by (24) to approximate the uncertain term* $f_1(\xi_v)$*, selects the adaptive law of (29) used to update the RBF neural network weight vector* $\widehat{W}$*, and constructs a sliding mode virtual controller of formulas (26) and (27); the dynamic pressure cylinder output pressure subsystem adopts the sliding mode switching function of (19), uses RBF neural network described by (31) to approximate the uncertain term* $f_2(\xi_p)$*, selects the adaptive law of (36) used to update the RBF neural network weight vector* $\widehat{P}$*, and constructs a backstepping sliding mode controller of formulas (33) and (34); both of the above subsystems can be consistently bounded at the end, so that the dynamic pressure cylinder electrohydraulic servo pressure system is gradually stabilized, and finally the output pressure tracking error of the system is converged.*

4.3.2. Stability Analysis. Discuss the stability of the dynamic pressure cylinder displacement subsystem and the dynamic pressure cylinder output pressure subsystem separately, and then we can evaluate the stability of the entire dynamic pressure cylinder electrohydraulic servo pressure system.

Proof. (1) Stability of the dynamic pressure cylinder displacement subsystem

Substituting the sliding mode adaptive virtual controller described in (27) for ξ_3 in (23), we can get

$$\dot{S_1} = f_1(\xi_v) - \widehat{W^T} h(\xi_v) - aa_3 K_1 sat\left(\frac{S_1}{\varphi_1}\right) \tag{37}$$

It can be known from Assumption 1 that

$$f_1(\xi_v) = Wb^T h(\xi_v) + \varepsilon_1 \tag{38}$$

(37) can be simplified to

$$\dot{S_1} = \widetilde{W^T} h(\xi_v) + \varepsilon_1 - aa_3 K_1 sat\left(\frac{S_1}{\varphi_1}\right) \tag{39}$$

where $\widetilde{W} = Wb - \widehat{W}$ is the RBF neural network weight vector estimation error and ε_1 is the approximation error of the RBF neural network for the uncertainty term $f_1(\xi_v)$.

Select the Lyapunov function:

$$V_1 = \frac{1}{2}S_1^2 + \frac{1}{2}\eta_1^{-1}\widetilde{W^T}\widetilde{W} \tag{40}$$

Taking the derivative of V_1 and substituting (39) into $\dot{V}_1$,

$$\begin{aligned} \dot{V}_1 &= S_1\dot{S}_1 - \eta_1^{-1}\widetilde{W^T}\dot{\widetilde{W}} \\ &= S_1\left(\widetilde{W^T}h(\xi_v) + \varepsilon_1 - aa_3K_1 sat\left(\frac{S_1}{\varphi_1}\right)\right) \\ &\quad - \eta_1^{-1}\widetilde{W^T}\dot{\widehat{W}} \end{aligned} \tag{41}$$

Substituting the RBF neural network weight vector adaptive law (29) into (41),

$$\dot{V}_1 = -aa_3K_1S_1 sat\left(\frac{S_1}{\varphi_1}\right) + \frac{\delta_1}{\eta_1}\widetilde{W^T}\widehat{W} + S_1\varepsilon_1 \tag{42}$$

From the Young inequality $a^T b \le (\lambda_{ab}/2)a^T a + (1/2\lambda_{ab})b^T b$, λ_{ab} is the normal number, and we can derive

$$S_1\varepsilon_1 \le \frac{\lambda w_1}{2}S_1^2 + \frac{1}{2\lambda w_1}\varepsilon_1^2 \tag{43}$$

$$\begin{aligned} \frac{\delta_1}{\eta_1}\widetilde{W^T}\widehat{W} &= \frac{\delta_1}{\eta_1}\widetilde{W^T}\left(Wb - \widetilde{W}\right) \\ &= \frac{\delta_1}{\eta_1}\widetilde{W^T}Wb - \frac{\delta_1}{\eta_1}\widetilde{W^T}\widetilde{W} \\ &\le -\frac{\delta_1}{\eta_1}\left(1 - \frac{\lambda w_2}{2}\right)\widetilde{W^T}\widetilde{W} + \frac{\delta_1}{2\lambda w_2 \eta_1}\|Wb\|^2 \end{aligned} \tag{44}$$

Discuss with the boundary function:

The adaptive law of switching gain K_1 is $\dot{K}_1 = K_{11}|S_1|$, and the coefficient K_{11} is a positive real number; we can know $\dot{K}_1 > 0$, so that $K_1 \ge 0$ can be obtained. $aa_3 = c_2a_3 > 0$; φ_1 is positive real number.

(a) When $|S_1| \le \varphi_1$, $K_1 sat(S_1/\varphi_1)S_1 = (K_1/\varphi_1)S_1^2$

$$\begin{aligned} \dot{V}_1 &= -\frac{aa_3K_1}{\varphi_1}S_1^2 + \frac{\delta_1}{\eta_1}\widetilde{W^T}\widehat{W} + S_1\varepsilon_1 \\ &\le -\left(\frac{aa_3K_1}{\varphi_1} - \frac{\lambda w_1}{2}\right)S_1^2 - \frac{\delta_1}{\eta_1}\left(1 - \frac{\lambda w_2}{2}\right)\widetilde{W^T}\widetilde{W} \\ &\quad + \frac{1}{2\lambda w_1}\varepsilon_1^2 + \frac{\delta_1\|Wb\|^2}{2\lambda w_2\eta_1} \\ &\le -K_{r1}S_1^2 - K_{w1}\widetilde{W^T}\widetilde{W} + \gamma_1 \le -K_{\lambda 1}V_1 + \gamma_1 \end{aligned} \tag{45}$$

where $K_{r1} = (aa_3K_1/\varphi_1 - \lambda w_1/2)$, $K_{w1} = (\delta_1/\eta_1)(1 - \lambda w_2/2)$, $K_{\lambda 1} = 2 * \min(K_{r1}, K_{w1})$, $\gamma_1 = (1/2\lambda w_1)\varepsilon_1^2 + \delta_1\|Wb\|^2/2\lambda w_2\eta_1$.

Select the parameters K_{r1} and K_{w1} being nonnegative real numbers, multiply by $e^{K_{\lambda 1}t}$ both sides of (45), and obtain the definite integral over the interval $[0, t]$:

$$V_1 = \left(V_1(0) - \frac{\gamma_1}{K_{\lambda 1}}\right) e^{-K_{\lambda 1}} t + \frac{\gamma_1}{K_{\lambda 1}} \tag{46}$$

When $t \longrightarrow \infty$, V_1 converges to $\gamma_1/K_{\lambda 1}$, all signals in the closed-loop system are uniformly bounded, and the tracking error is made as small as possible by selecting appropriate design parameters [26, 27].

(b) When $|S_1| > \varphi_1$, $K_1 sat(S_1/\varphi_1)S_1 = K_1 \mathrm{sgn}(S_1)S_1 = K_1|S_1| = (K_1/|S_1|)S_1^2$

$$\begin{aligned}
\dot{V}_1 &= -aa_3K_1\left|S_1\right| + \frac{\delta_1}{\eta_1}\widetilde{W^T}\widehat{W} + S_1\varepsilon_1 \\
&= -aa_3\frac{K_1}{\left|S_1\right|}S_1^2 + \frac{\delta_1}{\eta_1}\widetilde{W^T}\widehat{W} + S_1\varepsilon_1 \\
&\leq -\left(\frac{aa_3K_1}{\left|S_1\right|} - \frac{\lambda w_1}{2}\right)S_1^2 - \frac{\delta_1}{\eta_1}\left(1 - \frac{\lambda w_2}{2}\right)\widetilde{W^T}\widetilde{W} \\
&\quad + \frac{1}{2\lambda w_1}\varepsilon_1^2 + \frac{\delta_1\left\|Wb\right\|^2}{2\lambda w_2\eta_1} \\
&\leq -K_{r2}S_1^2 - K_{w1}\widetilde{W^T}\widetilde{W} + \gamma_1 \leq -K_{\lambda 2}V_1 + \gamma_1
\end{aligned} \tag{47}$$

where $K_{r2} = (aa_3K_1/|S_1| - \lambda w_1/2) \geq 0$, $K_{\lambda 2} = 2 * \min(K_{r2}, K_{w1})$.

we can obtain

$$V_1 = \left(V_1(0) - \frac{\gamma_1}{K_{\lambda 2}}\right) e^{-K_{\lambda 2}} t + \frac{\gamma_1}{K_{\lambda 2}} \tag{48}$$

All signals in the closed-loop system are consistently bounded.

To sum up,

$$V_1 = \begin{cases} \left(V_1(0) - \dfrac{\gamma_1}{K_{\lambda 1}}\right) e^{-K_{\lambda 1}} t + \dfrac{\gamma_1}{K_{\lambda 1}}, & \left|S_1\right| \leq \varphi_1 \\ \left(V_1(0) - \dfrac{\gamma_1}{K_{\lambda 2}}\right) e^{-K_{\lambda 2}} t + \dfrac{\gamma_1}{K_{\lambda 2}}, & \left|S_1\right| > \varphi_1 \end{cases} \tag{49}$$

The dynamic pressure cylinder displacement subsystem uses the adaptive RBF neural network of (24) and (29) to approximate the uncertain term $f_1(\xi_v)$, constructs the sliding mode virtual controller of (27), and selects the appropriate parameters; the system tracking error and the parameter approximation error can be ultimately bounded, and the closed-loop system eventually converges to a small neighborhood of zero.

(2) Stability of the dynamic pressure cylinder output pressure subsystem

Substituting the backstepping sliding mode adaptive controller (34) into (30), we get

$$\dot{S}_2 = f_2\left(\xi_p\right) - \widehat{P^T}\phi\left(\xi_p\right) - K_2aa_{11}g(u)\,sat\left(\frac{S_2}{\varphi_2}\right) \tag{50}$$

It is known by Assumption 2 that

$$f_2\left(\xi_p\right) = Pb^T\Phi\left(\xi_p\right) + \varepsilon_2 \tag{51}$$

(50) can be simplified to

$$\dot{S}_2 = \widetilde{P^T}\phi\left(\xi_p\right) + \varepsilon_2 - K_2aa_{11}g(u)\,sat\left(\frac{S_2}{\varphi_2}\right) \tag{52}$$

where $\widetilde{P} = Pb - \widehat{P}$ is the RBF neural network weight vector estimation error and ε_2 is the approximation error of the RBF neural network for the uncertainty term $f_2(\xi_p)$.

Design the Lyapunov function by referring to (13) to (21):

$$V_{51} = V_4 + \frac{1}{2}S_2^2 + \frac{1}{2}\eta_2^{-1}\widetilde{P^T}\widetilde{P} \tag{53}$$

Taking the derivative of V_{51} and substituting (53) into $\dot{V_{51}}$,

$$\begin{aligned}
\dot{V_{51}} &= \dot{V}_4 + S_2\dot{S}_2 - \eta_2^{-1}\widetilde{P^T}\dot{\widehat{P}} \\
&= -K_3K_4e_3^2 - K_3K_4K_5e_4^2 - K_3K_4e_4\left(e_4 - K_5e_5\right) \\
&\quad + S_2\left(\widetilde{P^T}\phi\left(\xi_p\right) + \varepsilon_2 - K_2aa_{11}g(u)\,sat\left(\frac{S_2}{\varphi_2}\right)\right) \\
&\quad - \eta_2^{-1}\widetilde{P^T}\dot{\widehat{P}}
\end{aligned} \tag{54}$$

Substituting the RBF neural network weight vector adaptive law (36) into (54),

$$\begin{aligned}
\dot{V_{51}} &= -K_3K_4e_3^2 - K_3K_4K_5e_4^2 - K_3K_4e_4\left(e_4 - K_5e_5\right) \\
&\quad - K_2aa_{11}g(u)\,S_2sat\left(\frac{S_2}{\varphi_2}\right) + \frac{\delta_2}{\eta_2}\widetilde{P^T}\widehat{P} + S_2\varepsilon_2
\end{aligned} \tag{55}$$

We can get by Young inequality that

$$S_2\varepsilon_2 \leq \frac{\lambda_{p1}}{2}S_2^2 + \frac{1}{2\lambda_{p1}}\varepsilon_2^2 \tag{56}$$

$$\begin{aligned}
\frac{\delta_2}{\eta_2}\widetilde{P^T}\widehat{P} &= \frac{\delta_2}{\eta_2}\widetilde{P^T}\left(Pb - \widetilde{P}\right) = \frac{\delta_2}{\eta_2}\widetilde{P^T}Pb - \frac{\delta_2}{\eta_2}\widetilde{P^T}\widetilde{P} \\
&\leq -\frac{\delta_2}{\eta_2}\left(1 - \frac{\lambda_{p1}}{2}\right)\widetilde{P^T}\widetilde{P} + \frac{\delta_2}{2\lambda_{p1}\eta_2}\left\|Pb\right\|^2
\end{aligned} \tag{57}$$

Let $0 < K_5 \le |e_4|/|e_5|$; we can get $-K_3K_4e_4(e_4 - K_5e_5) \le 0$, combined with (18); we know

$$\begin{aligned} \dot{V_4} &= -K_3K_4e_3^2 - K_3K_4K_5e_4^2 - K_3K_4e_4\left(e_4 - K_5e_5\right) \\ &\le -K_3K_4e_3^2 - K_3K_4K_5e_4^2 \end{aligned} \tag{58}$$

Discuss the following according to the definition of boundary function:

$\dot{K_2} = K_{22}|S_2|$ is the adaptive law of switching gain K_2, and by the coefficient K_{22} being a positive real number, we know $\dot{K_2} > 0$, so that $K_2 \ge 0$ can be obtained. It is known by (3) that $g(u) \ge 0$; $aa_{11} = C_5a_8 > 0$; φ_2 is positive real number.

(a) When $|S_2| \le \varphi_2$, $K_2 sat(S_2/\varphi_2)S_2 = (K_2/\varphi_2)S_2^2$

$$\begin{aligned} \dot{V_{51}} \le& -K_3K_4e_3^2 - K_3K_4K_5e_4^2 - \frac{K_2aa_{11}g(u)}{\varphi_2}S_2^2 \\ &+ \frac{\delta_2}{\eta_2}\widetilde{P^T}\widehat{P} + S_2\varepsilon_2 \\ \le& -K_3K_4e_3^2 - K_3K_4K_5e_4^2 - \frac{K_2aa_{11}g(u)}{\varphi_2}S_2^2 \\ &- \frac{\delta_2}{\eta_2}\left(1 - \frac{\lambda_{p1}}{2}\right)\widetilde{P^T}\widetilde{P} + \frac{\delta_2}{2\lambda_{p1}\eta_2}\|Pb\|^2 \\ &+ \frac{\lambda_{p1}}{2}S_2^2 + \frac{1}{2\lambda_{p1}}\varepsilon_2^2 \\ \le& -K_3K_4e_3^2 - K_3K_4K_5e_4^2 \\ &- \left(\frac{K_2aa_{11}g(u)}{\varphi_2} - \frac{\lambda_{p1}}{2}\right)S_2^2 + \frac{1}{2\lambda_{p1}}\varepsilon_2^2 \\ &- \frac{\delta_2}{\eta_2}\left(1 - \frac{\lambda_{p1}}{2}\right)\widetilde{P^T}\widetilde{P} + \frac{\delta_2}{2\lambda_{p1}\eta_2}\|Pb\|^2 \\ \le& V_4 - K_{r3}S_1^2 - K_{p1}\widetilde{P^T}\widetilde{P} + \gamma_2 \le -K_{\lambda 3}V_{51} + \gamma_2 \end{aligned} \tag{59}$$

where $K_{r3} = K_2aa_{11}g(u)/\varphi_2 - \lambda_{p1}/2$, $K_{\lambda 3} = 2 * \min(K_{r3}, K_{p1})$, $\gamma_2 = (1/2\lambda_{p1})\varepsilon_2^2 + (\delta_2/2\lambda_{p1}\eta_2)\|Pb\|^2$, $K_{p1} = (\delta_2/\eta_2)(1 - \lambda_{p1}/2)$.

Select the parameters K_{r3} and K_{p1} being nonnegative real numbers, multiply by $e^{K_{\lambda 3}t}$ both sides of (59), and obtain the definite integral over the interval $[0, t]$:

$$V_{51} = \left(V_{51}(0) - \frac{\gamma_2}{K_{\lambda 3}}\right)e^{-K_{\lambda 3}}t + \frac{\gamma_2}{K_{\lambda 3}} \tag{60}$$

When $t \longrightarrow \infty$, V_{51} converges to $\gamma_2/K_{\lambda 3}$, all signals in the closed-loop system are uniformly bounded, and designing $K_{\lambda 3} \gg \gamma_2$ ensures that the closed-loop system eventually converges to a small neighborhood of zero.

(b) When $|S_2| > \varphi_2$, $K_2 sat(S_2/\varphi_2)S_2 = K_2|S_2| = (K_2/|S_2|)S_2^2$

$$\begin{aligned} \dot{V_{51}} \le& -K_3K_4e_3^2 - K_3K_4K_5e_4^2 - \frac{K_2aa_{11}g(u)}{|S_2|}S_2^2 \\ &+ \frac{\delta_2}{\eta_2}\widetilde{P^T}\widehat{P} + S_2\varepsilon_2 \\ \le& -K_3K_4e_3^2 - K_3K_4K_5e_4^2 - \frac{K_2aa_{11}g(u)}{|S_2|}S_2^2 \\ &- \frac{\delta_2}{\eta_2}\left(1 - \frac{\lambda_{p1}}{2}\right)\widetilde{P^T}\widetilde{P} + \frac{\delta_2}{2\lambda_{p1}\eta_2}\|Pb\|^2 \\ &+ \frac{\lambda_{p1}}{2}S_2^2 + \frac{1}{2\lambda_{p1}}\varepsilon_2^2 \\ \le& -K_3K_4e_3^2 - K_3K_4K_5e_4^2 \\ &- \left(\frac{K_2aa_{11}g(u)}{|S_2|} - \frac{\lambda_{p1}}{2}\right)S_2^2 + \frac{1}{2\lambda_{p1}}\varepsilon_2^2 \\ &- \frac{\delta_2}{\eta_2}\left(1 - \frac{\lambda_{p1}}{2}\right)\widetilde{P^T}\widetilde{P} + \frac{\delta_2}{2\lambda_{p1}\eta_2}\|Pb\|^2 \\ \le& V_4 - K_{r4}S_1^2 - K_{p1}\widetilde{P^T}\widetilde{P} + \gamma_2 \le -K_{\lambda 4}V_{51} + \gamma_2 \end{aligned} \tag{61}$$

where $K_{r4} = K_2aa_{11}g(u)/|S_2| - \lambda_{p1}/2$, $K_{\lambda 4} = 2 * \min(K_{r4}, K_{p1})$.

we can get

$$V_{51} = \left(V_{51}(0) - \frac{\gamma_2}{K_{\lambda 4}}\right)e^{-K_{\lambda 4}}t + \frac{\gamma_2}{K_{\lambda 4}} \tag{62}$$

All signals in a closed-loop system are consistently bounded.

To sum up,

$$V_{51} = \begin{cases} \left(V_{51}(0) - \dfrac{\gamma_2}{K_{\lambda 3}}\right)e^{-K_{\lambda 3}}t + \dfrac{\gamma_2}{K_{\lambda 3}}, & |S_2| \le \varphi_2 \\ \left(V_{51}(0) - \dfrac{\gamma_2}{K_{\lambda 4}}\right)e^{-K_{\lambda 4}}t + \dfrac{\gamma_2}{K_{\lambda 4}}, & |S_2| > \varphi_2 \end{cases} \tag{63}$$

The dynamic pressure cylinder output pressure subsystem uses the adaptive RBF neural network of (31) and (36) to approximate the uncertain term $f_2(\xi_p)$ and, through constructing the backstepping sliding mode controller of (34), selects the appropriate parameters to make the system tracking error and the parameter approximation error ultimately bounded, thus ensuring that the closed-loop system eventually converges to a small neighborhood of zero.

(3) Stability of the dynamic pressure cylinder electrohydraulic servo pressure system

Based on the discussion of the stability of the above two subsystems, the final Lyapunov function of the design system is expressed as

$$V_6 = V_1 + V_{51} \tag{64}$$

Table 1: Parameters of AMESim model for dynamic pressure cylinder electro-hydraulic servo pressure system.

Component	Parameter	value
Hydraulic oil	Density/Kg·m^{-3}	850
	absolute viscosity/Pa·s	0.028
	Bulk modulus /MPa	900
Hydraulic source	Pressure source /MPa	20.6
	Flow source /L·min^{-1}	200
Servo valve	Rated current /mA	40
	Natural frequency/Hz	80
	Maximum flow /L·min^{-1}	120
Dynamic pressure cylinder	Piston diameter/mm	125
	Rod diameter/mm	90
	Cylinder stroke/mm	50
Load	Elastic stiffness /N·m^{-1}	1.53×10^{8}
	Mass /Kg	200

The derivative of V_6 is

$$\dot{V_6} = \dot{V_1} + \dot{V_{51}} \leq -K_\lambda V_6 + \gamma \tag{65}$$

where $K_\lambda = \min(K_{\lambda 1}, K_{\lambda 2}, K_{\lambda 3}, K_{\lambda 4})$, $\gamma = \gamma_1 + \gamma_2$. Further, we can get

$$V_6 = \left(V_6(0) - \frac{\gamma}{K_\lambda} \right) e^{-K_\lambda} t + \frac{\gamma}{K_\lambda} \tag{66}$$

It can be seen that Theorem 3 can make the tracking error and parameter approximation error of the dynamic pressure cylinder electrohydraulic pressure system bounded, thus ensuring the stable convergence of the closed-loop system.

Proof completed. □

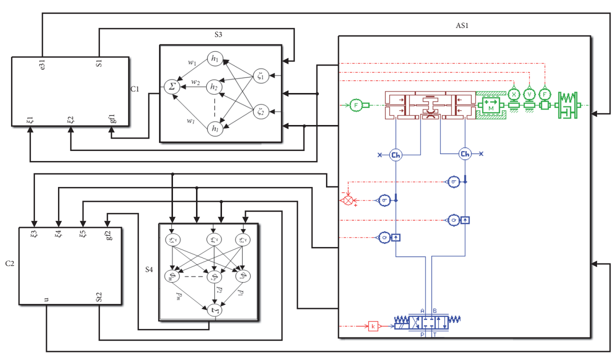

Figure 4: Dynamic pressure cylinder electrohydraulic servo pressure system RBF neural network backstepping sliding mode adaptive control AMESim and Simulink cosimulation block diagram.

5. Simulation Research

Based on the dynamic pressure cylinder servo pressure system described in (7), according to Theorem 3, the AMESim and Simulink cosimulation block diagram of RBF neural network backstepping sliding mode adaptive control is constructed as in Figure 4.

In Figure 4, AS1 is the AMESim model of the dynamic pressure cylinder electrohydraulic servo pressure system, and its parameters settings are shown in Table 1. C1 is the sliding mode adaptive controller of the dynamic pressure cylinder displacement subsystem, and S3 is the RBF neural network approximator of the displacement subsystem uncertainty term. C1 and S3 constitute the dynamic pressure cylinder displacement subsystem RBF neural network sliding mode adaptive control. C2 is the backstepping sliding mode adaptive controller of the dynamic pressure cylinder output pressure subsystem, S4 is the RBF neural network approximator of the output pressure subsystem uncertainty item. C2 and S4 constitute the dynamic pressure cylinder output pressure subsystem RBF neural network backstepping sliding mode adaptive control. Finally, through the virtual controller e31 and the dynamic pressure cylinder output pressure controller u, realize the dynamic pressure cylinder electrohydraulic servo pressure system RBF neural network backstepping sliding mode adaptive control.

Select the target variable $P_r = 1.7e^7 \sin(20\pi t)$Pa, and the expected deviation of the output pressure deviation ξ_3 is $\xi_{d3} = 0$; we can refer to (22) to derive the approximate dynamic pressure cylinder expected displacement ξ_{d1}, and set the parameters of the backstepping sliding mode adaptive controller according to Table 2.

The dynamic pressure cylinder displacement subsystem RBF neural network is designed as a 2-11-1 structure, containing 11 neurons; i.e., $l = 11$. The first set of 11 network node center vectors $[C_{11}, C_{12}, \ldots, C_{111}]$ of the input variable ξ_1 are evenly distributed in the $0.15 * [-2, 2]$ region, and the other set of 11 network node center vectors $[C_{21}, C_{22}, \ldots, C_{211}]$ of the input variable ξ_2 are evenly distributed in the $4 * [-2, 2]$ region. The network node base width parameter is $b = 0.5 *$ ones$(11, 1)$.

The dynamic pressure cylinder output pressure subsystem RBF neural network is designed as a 3-16-1 structure, containing 16 neurons; i.e., m=16. The first set of 16 network node center vectors $[CP_{11}, CP_{12}, \ldots, CP_{116}]$ of the input

Table 2: Backstepping sliding mode adaptive controller parameters.

Parameter	value	Parameter	value
c_1	1e-1	c_2	1e-2
c_3	1e-2	c_4	1e-6
c_5	6.8e-9	K_{11}	5.1e1
K_{22}	1.8	K_3	1e-4
K_4	1e-5	K_5	1e-6
φ_1	2e-1	φ_2	3e2
η_1	5e3	η_2	3.5e5

variable ξ_3 are evenly distributed in the $1.7e7 * [-2, 2]$ region, the second set of 16 network node center vectors $[CP_{21}, CP_{22}, \ldots, CP_{216}]$ of the input variable ξ_4 are evenly distributed in the $1e9 * [-2, 2]$ region, and the third set of 16 network node center vectors $[CP_{31}, CP_{32}, \ldots, CP_{316}]$ of the input variable ξ_5 are evenly distributed in the $1.1e11 * [-2, 2]$ region. Network node base width parameters are $bp(1) = 2e7 * \text{ones}(16, 1)$, $bp(2) = 1e9 * \text{ones}(16, 1)$, $bp(3) = 1e11 * \text{ones}(16, 1)$.

Carry out the AMESim and Simulink cosimulation of the dynamic pressure cylinder electrohydraulic servo pressure system RBF neural network backstepping sliding mode adaptive control. The performance simulation curves are shown in Figure 5.

Figures 5(a) and 5(b) are, respectively, the contrast curves of the dynamic pressure cylinder AMESim model RBF neural network backstepping sliding mode adaptive control (RBFNNBSAC) and backstepping sliding mode adaptive control (BSAC) output pressure and their deviations. Compared with the backstepping sliding mode adaptive control (BSAC), the RBF neural network backstepping sliding mode adaptive control (RBFNNBSAC) has a short dynamic response time and no overshoot, and the output pressure deviation amplitude is only 3.1e-3 (about 5.3e4Pa) of the set pressure amplitude, about 70% of the BSAC output pressure deviation amplitude (about 7.4e4Pa), showing that the RBF neural network backstepping sliding mode adaptive control has better dynamic and static performance.

The comparison curves of the outputs of RBFNNBSAC and BSAC controller are shown in Figure 5(c). Compared with the output u of the BSAC controller, the output of the RBFNNBSAC controller u_1 has a short adjustment time, fast convergence, and smooth curve, so that better control performance can be achieved.

In Figure 5(d), the virtual control variable e_{31} is much larger than the output pressure e_3, although there is a large deviation, because the stabilities of the two subsystems are independent of each other, and therefore the whole system is still stable.

Figures 5(e) and 5(f) are, respectively, the RBF neural network adaptive estimation curves for the dynamic pressure cylinder displacement subsystem uncertainty item f_1 and the dynamic pressure cylinder output pressure subsystem uncertainty item f_2, the approximation curves are stable and bounded, and the output of the controller u_1 can be adjusted in real time to reduce the influence of parameter uncertainty on the tracking performance of the dynamic pressure cylinder output pressure.

Further, at 1.5s, a sinusoidal interference signal (0.2 sin (20 pi∗t), lasting 1 s) is applied to the RBF neural network backstepping sliding mode adaptive controller output u_1, and the interference response curve is as shown in Figure 6.

Figure 6(a) shows the good anti-jamming performance of the RBFNNBSAC control system. Figures 6(b) and 6(c) show more directly the changes in output pressure tracking deviation during the whole process of interference generation and disappearance: although the interference makes the amplitude of the output pressure deviation larger, its max amplitude is only 7.9e-3 (about 1.3e5Pa) of the set pressure amplitude, still having high tracking accuracy, and the output pressure deviation can be rapid return to the pre-interference level after the interference disappears.

The output of the RBFNNBSAC controller in Figure 6(d) can be adjusted according to the interference signal, and after the interference disappears, the output size of controller can be restored. Uncertainty terms f_1 and f_2 RBFNN approximation of the interference response curves are shown in Figures 6(e) and 6(f); the interference still has no effect on the uncertainty f_1 RBFNN approximation curve, but the uncertain term f_2 RBFNN approximation curve can quickly and sensitively respond to the interference signal, adjusting the compensation of the RBFNN approximation network to the interference signal in real time.

The target variable P_r is set to triangle wave and square wave signal with amplitude 1.7e7Pa and frequency 10Hz, respectively, and modifies some parameters of RBF neural network backstepping sliding mode adaptive controller; the simulation curves of the RBF neural network backstepping sliding mode adaptive control based on dynamic pressure cylinder AMESim model are, respectively, shown in Figures 7 and 8.

From Figures 7(a)–7(c) and Figures 8(a)–8(c), it can be seen that the RBF neural network backstepping sliding mode adaptive control (RBFNNBSAC) can also effectively track triangular and square wave signals. There are some certain tracking errors; however, compared with the backstepping sliding mode adaptive control (BSAC), the algorithm has good dynamic and static control performances (fast response, small overshoot, small steady-state error, etc.), and the demand of control performance of dynamic pressure cylinder electrohydraulic servo pressure system can be satisfied.

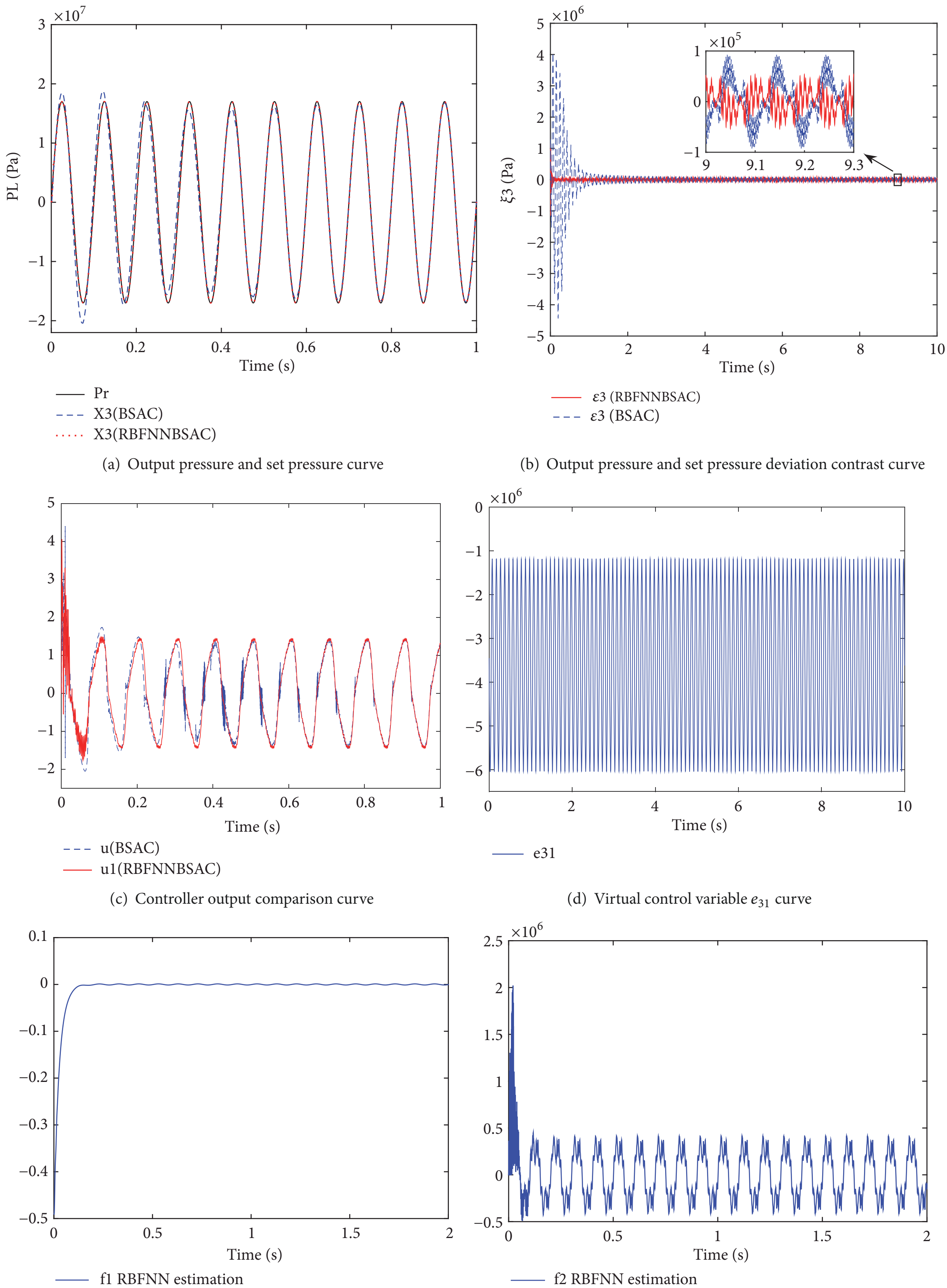

(a) Output pressure and set pressure curve

(b) Output pressure and set pressure deviation contrast curve

(c) Controller output comparison curve

(d) Virtual control variable e_{31} curve

(e) Uncertainty term f_1 RBFNN approximation curve

(f) Uncertainty term f_1 RBFNN approximation curve

FIGURE 5: Performance curve of dynamic pressure cylinder AMESim model RBF neural network backstepping sliding mode adaptive control (10Hz sine).

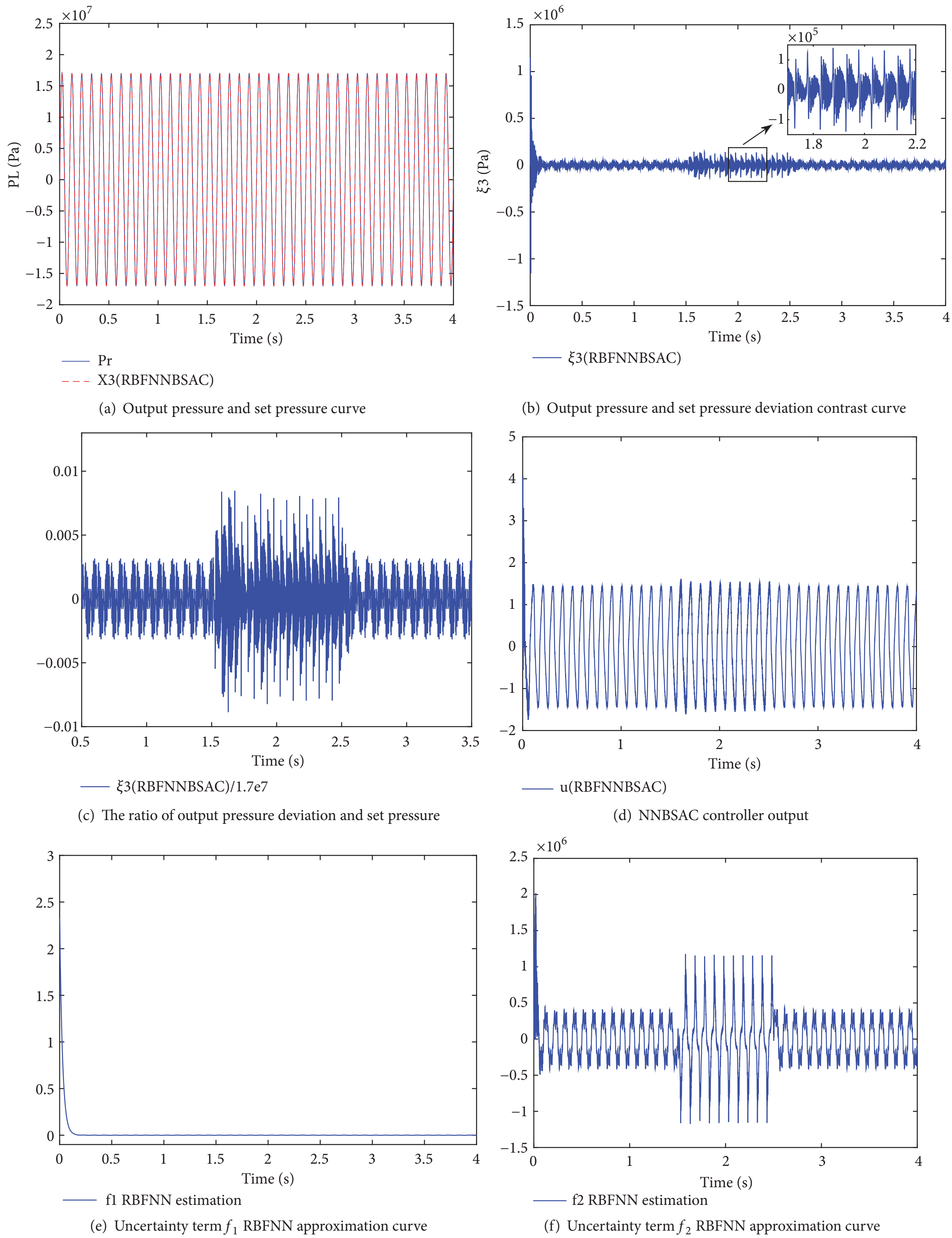

(a) Output pressure and set pressure curve

(b) Output pressure and set pressure deviation contrast curve

(c) The ratio of output pressure deviation and set pressure

(d) NNBSAC controller output

(e) Uncertainty term f_1 RBFNN approximation curve

(f) Uncertainty term f_2 RBFNN approximation curve

FIGURE 6: Dynamic pressure cylinder AMESim model RBF neural network backstepping sliding mode adaptive control interference response curve (10Hz sine).

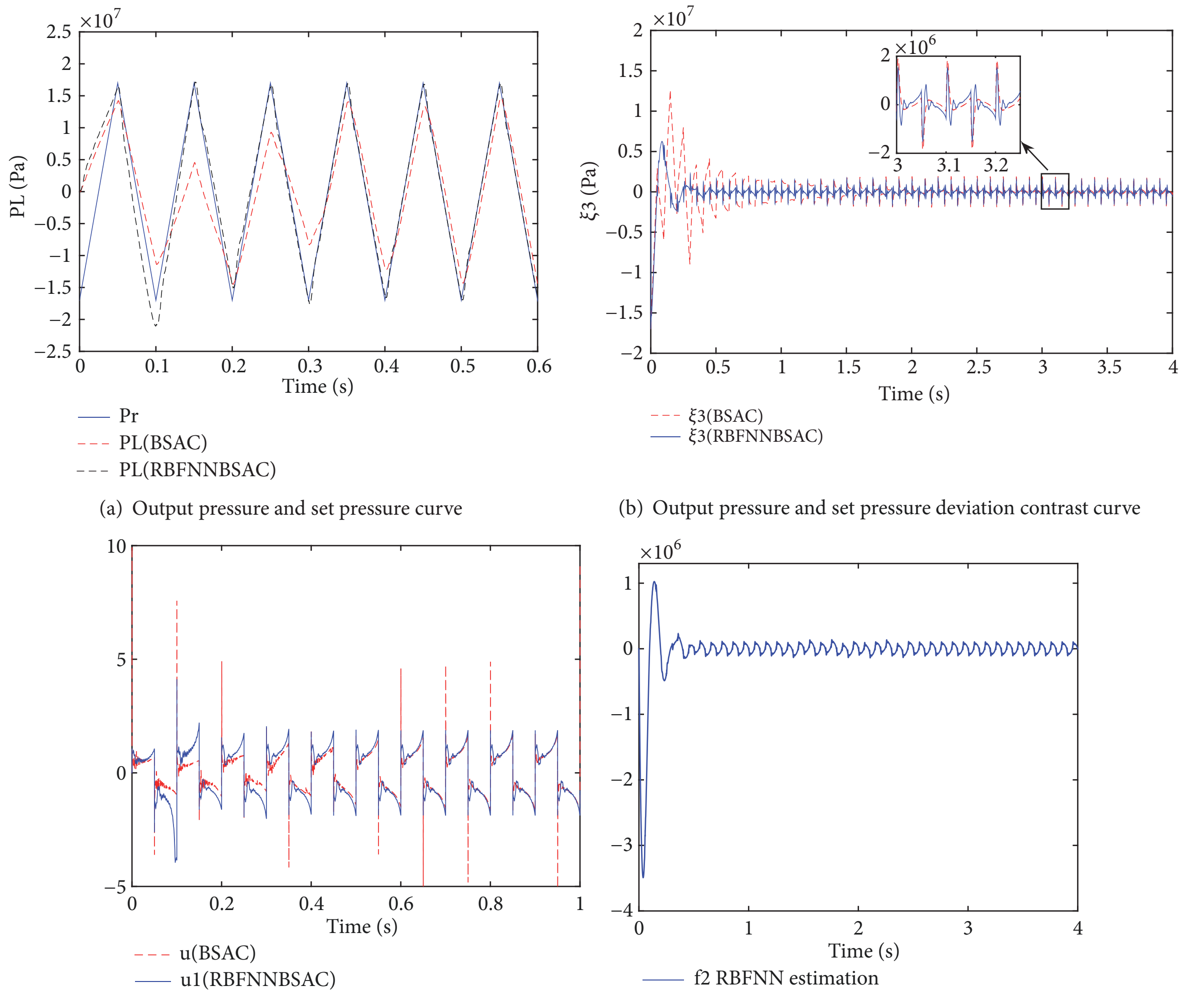

(a) Output pressure and set pressure curve

(b) Output pressure and set pressure deviation contrast curve

(c) RBFNNBSAC controller output

(d) Uncertainty term f_2 RBFNN approximation curve

Figure 7: Performance curve of dynamic pressure cylinder AMESim model RBF neural network backstepping sliding mode adaptive control (10Hz triangle wave).

6. Conclusion

Based on the backstepping sliding mode adaptive control of the dynamic pressure cylinder, the RBF neural networks are introduced to approximate the uncertain terms f_1 and f_2. According to the double sliding surface, the RBF neural network weight vector adaptive laws of the displacement subsystem and the output pressure subsystem are, respectively, constructed, thus realizing the automatic updates of the displacement subsystem virtual controller e_{31} and the output pressure subsystem backstepping sliding mode controller u, reducing the difficulty of controller design.

Target variable $P_r = 1.7e^7 \sin(20\pi t)$Pa is set, the RBF neural network backstepping sliding mode adaptive algorithm is applied to the dynamic pressure cylinder AMESim model, and the control performances of the algorithm are simulated and analyzed. The results show that, compared with the backstepping sliding mode adaptive control (BSAC), the RBFNNBSAC algorithm has better dynamic and static performances and tracking performances, and it can effectively track the target expected variable P_r. Further, an interference signal is applied to the dynamic pressure cylinder, and the uncertainty term f_2 RBFNN can quickly respond to the change of the interference signal, continuously adjusting the compensation amount of the RBFNN to the interference signal, so that the controller output u adaptive responded to the change of the interference signal, greatly reducing the influence of the interference signal on the tracking error, and had better anti-interference ability.

Finally, the triangular and square wave signals with amplitude 1.7e7Pa and frequency 10Hz are applied to the dynamic pressure cylinder AMESim model; the algorithm (RBFNNBSAC) and the backstepping sliding mode adaptive (BSAC) are simulated by contrast curves. It is found that RBFNNBSAC has better dynamic and static performances, and the control output is unsaturated and smoother, which can better track the desired pressure signal.

In future, we plan to apply the RBFNN backstepping sliding mode adaptive control algorithm to experimental platform of the track subgrade test device, and further

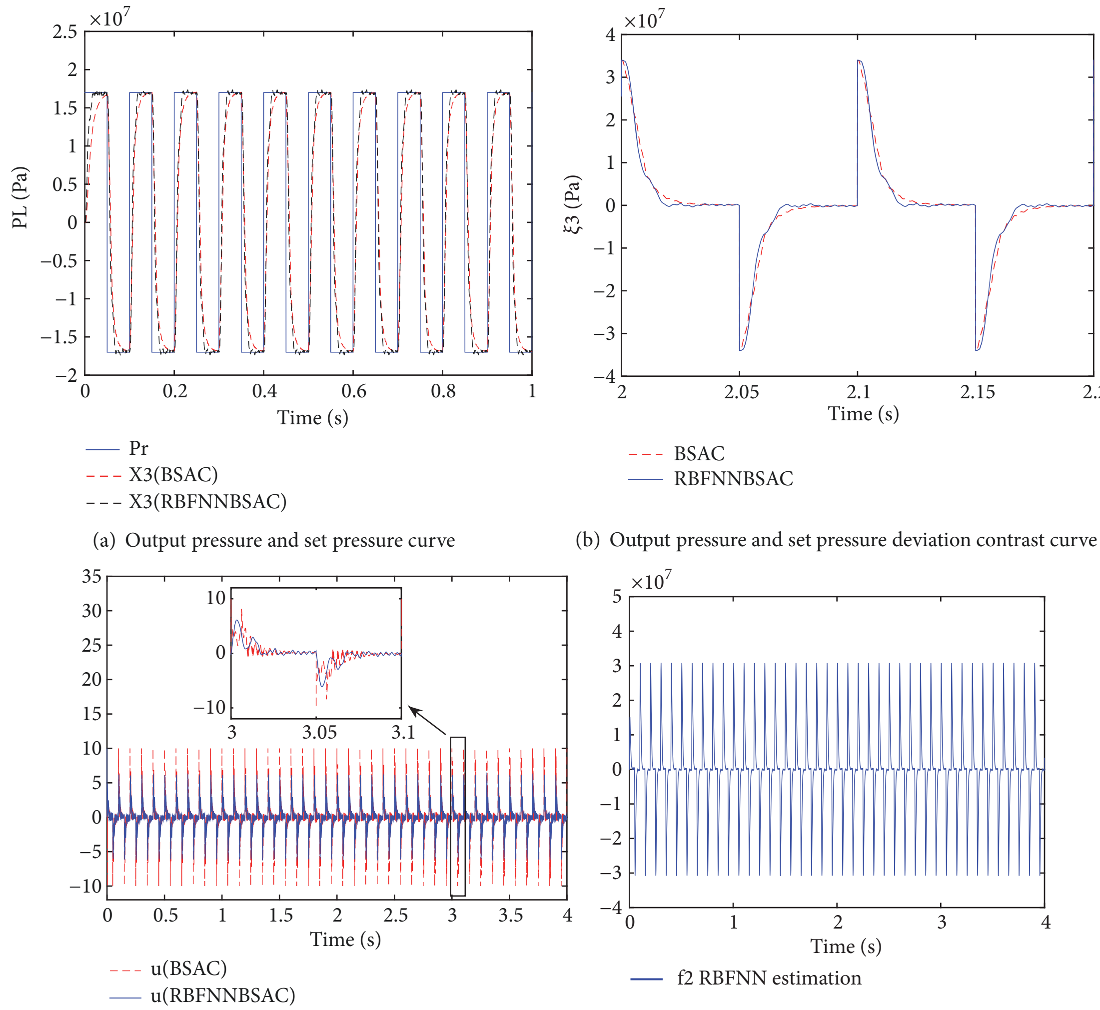

(a) Output pressure and set pressure curve

(b) Output pressure and set pressure deviation contrast curve

(c) RBFNNBSAC controller output

(d) Uncertainty term f_2 RBFNN approximation curve

Figure 8: Performance curve of dynamic pressure cylinder AMESim model RBF neural network backstepping sliding mode adaptive control (10Hz square wave).

optimize the control algorithm to improve the control performance of the device.

Data Availability

The readers can access the data used in this paper by contacting the corresponding author.

Conflicts of Interest

The authors declare that there are no conflicts of interest regarding the publication of this paper.

Acknowledgments

This work was partially supported by the National Natural Science Foundation of China (51027002) and Wuhan Branch of Baosteel Central Research Institute (R&D Center of Wuhan Iron & Steel Co., Ltd.) of China Baowu Steel Group Corporation Limited [grant number K18BWBCA50].

References

[1] L. Zeng, C. Chen, and X. Chen, "Design of Hydraulic Excitation System for Dynamic Response Testing of Railway Subgrade," *Chinese Hydraulics & Pneumatics*, vol. 4, pp. 9-10, 2012.

[2] Peng. Li, X. Chen, Y. Wan et al., "Research on Pressure Servo valve of Rail Track Dynamic Test Excitation System," *Chinese Hydraulics & Pneumatics*, vol. 8, pp. 62–65, 2013.

[3] Pan. Deng, Liu. Yang, and Li. Hua, "Integrated sliding mode adaptive control for the dynamic pressure cylinder electro-hydraulic servo pressure control system based on AMESim," *Chinese Hydraulics Pneumatics*, vol. 7, pp. 88-89, 2018.

[4] Y. Fang, J. Qi, J. Li et al., "Backstepping sliding mode control for continuous cast mold displacement system driven by electro-hydraulic servo system," *Electric Machines and Control*, vol. 18, no. 4, pp. 97-98, 2014.

[5] L. Liu, Z. Li, Y.-M. Fang, and J.-X. Li, "Sliding-mode control of continuous cast Mold oscillation displacement system driven by servo motor," *Dianji yu Kongzhi Xuebao/Electric Machines and Control*, vol. 20, no. 12, pp. 101–108, 2016.

[6] L. Zhou, C.-S. Jiang, and Y.-L. Du, "A robust and adaptive terminal sliding mode control based on backstepping," *Kongzhi Lilun Yu Yingyong/Control Theory and Applications*, vol. 26, no. 6, pp. 678–682, 2009.

[7] S. Duan, G. An, J. Xue, J. Wu, M. Wang, and T. Lin, "Adaptive sliding mode control for electrohydraulic servo force control systems," *Jixie Gongcheng Xuebao/Chinese Journal of Mechanical Engineering*, vol. 38, no. 5, pp. 109–113, 2002.

[8] J. d. Rubio, E. Garcia, G. Aquino, C. Aguilar-Ibañez, J. Pacheco, and A. Zacarias, "Learning of operator hand movements via least angle regression to be teached in a manipulator," *Evolving Systems*, vol. 2, pp. 1–16, 2018.

[9] Y. Pan, Y. Liu, B. Xu, and H. Yu, "Hybrid feedback feedforward: An efficient design of adaptive neural network control," *Neural Networks*, vol. 76, pp. 122–134, 2016.

[10] Y. Pan and H. Yu, "Biomimetic hybrid feedback feedforward neural-network learning control," *IEEE Transactions on Neural Networks and Learning Systems*, vol. 28, no. 6, pp. 1481–1487, 2017.

[11] X.-f. Su, "Adaptive Backstepping Sliding Mode Control for PMSM Position Servo System," *Small Special Electrical Machines*, vol. 39, no. 4, pp. 46–49, 2011.

[12] C.-T. Liu, B. Li, and Z.-x. He, "Sliding Mode Control of Theodolite Axis Servo System," *Computer Simulation*, vol. 32, no. 6, pp. 296–301, 2015.

[13] P. Fu, Z. Chen, B. Cong, and J. Zhao, "A position servo system of permanent magnet synchronous motor based on back-stepping adaptive sliding mode control," *Diangong Jishu Xuebao/Transactions of China Electrotechnical Society*, vol. 28, no. 9, pp. 288–301, 2013.

[14] G.-Q. Li, Y.-S. Gu, J. Li, Y.-S. Li, and B.-J. Guo, "Adaptive Backstepping Sliding Mode Control of Passive Electro-hydraulic Force Servo System," *Binggong Xuebao/Acta Armamentarii*, vol. 38, no. 3, pp. 616–624, 2017.

[15] X. Shao, L. Zhu, and Y. Liu, "SMDO-based backstepping terminal sliding mode control method for hot press hydraulic position servo system," in *Proceedings of the 27th Chinese Control and Decision Conference, CCDC 2015*, pp. 596–601, China, May 2015.

[16] Y. Fang, Z. Jiao, W. Wang et al., "Adaptive backstepping sliding mode control for rolling mill hydraulic servo position system," *Electric Machines and Control*, vol. 15, no. 10, pp. 95–100, 2011.

[17] Y. Sun, W. G. Zhang, and M. Zhang, "Adaptive sliding mode high maneuver flight control based on backstepping procedure," *Kongzhi yu Juece/Control and Decision*, vol. 26, no. 9, pp. 1377–1381, 2011.

[18] Y. Liao, J Zhuang, and Y. Pang, "Backstepping adaptive sliding mode control for an unmanned planning craft course system with single waterjet," *CAAI Transactions on Intelligent Systems*, vol. 3, no. 7, pp. 246–250, 2012.

[19] C. Xu and Y. Wang, "Nonsingular terminal neural network sliding mode control for manipulator joint based on backstepping," *Jixie Gongcheng Xuebao/Journal of Mechanical Engineering*, vol. 48, no. 23, pp. 36–40, 2012.

[20] Z.-Y. Chen, H.-J. Wang, X.-Q. Bian, and H.-M. Jia, "Stable neural network backstepping for diving control of AUV based on feedback gain," *Kongzhi yu Juece/Control and Decision*, vol. 28, no. 3, pp. 407–412, 2013.

[21] Wan Y., L. Zeng, and W. Li, "Design and Simulation for Hydraulic System of Excitation Device of High-speed Rail Track Dynamic Test System," *Machine Tool & Hydraulics*, vol. 40, no. 21, pp. 94–98, 2012.

[22] C. Guan and S. Zhu, "Backstepping-based multiple cascade adaptive sliding mode control of an electro-hydraulic servo system," *Yi Qi Yi Biao Xue Bao/Chinese Journal of Scientific Instrument*, vol. 26, no. 6, pp. 569–573, 2005.

[23] J.-K. Liu and F.-C. Sun, "Research and development on theory and algorithms of sliding mode control," *Control Theory & Applications*, vol. 24, no. 3, pp. 407–411, 2007.

[24] X. J. Chang, L. Liu, and R. X. Cui, "A nonsingular fast terminal sliding mode controller with varying boundary layers for permanent magnet synchronous motors," *Xi'an Jiaotong Daxue Xuebao. Journal of Xi'an Jiaotong University*, vol. 49, no. 6, pp. 53–59, 2015.

[25] H.-Q. Duan and H.-F. Sun, "Adaptive backstepping neural network algorithm of ship line-course control," *Nanjing Li Gong Daxue Xuebao/Journal of Nanjing University of Science and Technology*, vol. 36, no. 3, pp. 427–431, 2012.

[26] K. K. Hassan, *Nonlinear systems*, America Prentiee Hall, 3rd edition, 2002.

[27] C. Daizhan, *Applied Nonlinear Control*, China Machine Press, Beijing, China, 2006.